Instron® Corporation
825 University Avenue ■ Norwood, MA 02062-2643
Tel: +1-781-828-2500 ■ Fax: +1-781-575-5750
www.instron.com

Drop Impact: Fundamentals and Impact Characterisation of Solder Joints

E.H. Wong[1,2], R. Rajoo[1], Y.W. Mai[2], S.K.W. Seah[3], K.T. Tsai[4], L.M. Yap[4]
[1] Institute of Microelectronics, eehua@ime.a-star.edu.sg
[2] University of Sydney, Centre for Advanced Materials Technology
[3] National University of Singapore, Dept of Mechanical & Production Engineering
[4] Instron Singapore Pte Ltd

Abstract

This paper presents a summary of the fundamental theories behind board level drop impact covering the dynamics of drop impact assembly, dynamics of PCB, as well as interconnection stress. This is followed by a comprehensive study of the fracture characteristics of solder interconnections under high-speed impact using a newly developed Instron Micro Impactor which provides both the fracture strength as well as fracture energy of impact. The test matrix consists of five solder alloys, four pad finishing, three thermal histories, and two solder mask designs forming a total of 120 combinations. The test has highlighted weakness in NSMD design and caution on SnAgCu solder when used in drop impact application.

1. Introduction

Miniaturisation of portable electronic products has contributed to the vulnerability of board level interconnections to drop impact. This has prompted a new JEDEC board level drop impact test standard [1]. Drop experiments at the product level have provided useful understanding of the dynamic response of the PCB as a function of product type and impact angle [2-4]. Numerical simulation [5] and experimental validation [6,7] has confirmed differential flexing between the PCB and the IC packages as the primary driver for the failure of board level interconnections in drop impact. Computational models have been used extensively to model the dynamics of the PCB as well as the interconnection stresses due to board level drop impact [8-10, 5]. Analytical solutions that provide physical insights to the dynamics of PCB [11] and the interconnection stresses have also been presented [12,5,6].

High strain rate tends to raise the fracture toughness of ductile materials while lowers the fracture toughness of brittle materials [13]. Thus, the reliability of interconnections at drop impact will be governed more by the fracture toughness of the brittle intermetalics than by its bulk creep strength, as in the case of temperature cycling. It follows that the solder alloys and pad finishing that are ideal for temperature cycling may not be ideal for drop impact. While JEDEC prescribed board level drop test standard may be used to evaluate the impact performance of solders and pad finishing, it is a very costly test and the shock and noise accompanying the test can be extremely annoying. Simpler and cheaper tests have been explored for investigating the impact performance of interconnection joint, with potential as a routine quality control test in component manufacturing environment. Component level impact shear tests have been reported using split Hopkinson bar technique [14] as well as miniature Charpy test [15]. The former has reported inferior impact fracture strength of SnAgCu solder compared to eutectic SnPb solder while the later has reported superior impact fracture energy of the SnAgCu solder.

This paper presents a summary of the fundamental theories behind the board level drop impact test, follows by a comprehensive study of the characteristics of solder interconnects under high speed impact using a newly developed Instron Micro Impactor which provides both the fracture strength as well as fracture energy of impact.

Drop Impact: Fundamentals and Impact Characterisation of Solder Joints (cont.)

2. Fundamental Mechanics of Board Level Drop Impact

2.1 Dynamics of Drop Impact Test Assembly

Fig 1a illustrates a typical board level drop test. In the typical drop impact test, the base structure is prescribed with a half-sine acceleration pulse of a defined amplitude and duration. In the experimental set-up, this prescribed acceleration pulse is achieved by manipulating the fall height and the stiffness of the shock pad – This is usually carried out haphazardly. An understanding of the mechanics of this event will be useful for the conduct of the experiment. This can be achieved by modeling the drop assembly together with the shock pad simplistically as a combination of two spring-mass systems as illustrated in Fig 1b.

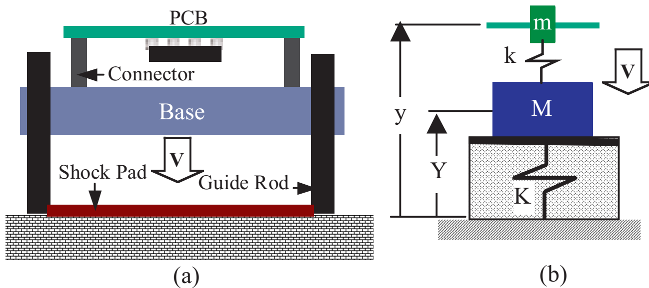

Figure 1: Typical board level drop impact (a) schematic (b) modelled as 2 spring-mass systems

where m and k are the representative mass and stiffness of the PCB respectively; M is the mass of the base structure, and K is the stiffness of the shock pad. The equation of motion of the system is given by eq(1)

$$m\ddot{y} + ky - kY = 0 \qquad (1)$$
$$M\ddot{Y} - ky + (k+K)Y = 0$$

and the frequencies of the system can be shown to be given by

$$\omega^4 - \frac{m(k+K)+Mk}{mM}\omega^2 + \frac{kK}{mM} = 0 \qquad (2)$$

For a typical board level drop impact set up, K»k and eq(2) is reduced to

$$\omega^2, \Omega^2 \approx \frac{k}{m}, \frac{K}{M} \qquad (3)$$

For the initial conditions $y(0)=Y(0)=0$ and $y(0)=Y(0)=-V_o$, as in the case of a board level drop impact, the solutions to the equations of motion for the base can be shown to be

$$Y(t) = \frac{V_o}{\Omega}\sin\Omega t \qquad (4)$$

and its acceleration expressed in terms of K, M, and the free-fall height H is given by

$$A_o = \sqrt{\frac{2gH.K}{M}}, \quad t_o = \pi\sqrt{\frac{M}{K}} \qquad (5)$$

It becomes clear that in carrying out the board level drop impact experiment, one shall first select the shock pad with the appropriate stiffness to produce the desired duration for base acceleration, follow by varying the free-fall height to produce the desired amplitude of base acceleration.

2.2 Dynamics of PCB

The base structure and the connectors are typically made of metal whose longitudinal stiffness is much higher than the flexural stiffness of the PCB. The half-sine acceleration pulse will therefore transmit to the PCB through the base and the connectors with little distortion. As such, the analysis of a board level drop impact may be reduced to modeling the PCB alone subjected to the half-sine acceleration pulse applied at its points of mounting to the connectors.

The dynamics of the PCB subjected to a half-sine acceleration pulse applied at its support may be analysed by modelling the PCB as an Euler-Bernoulli beam simply supported at its ends as depicted in Fig 2. The equation of motion is given by eq (6)

$$\ddot{w}(x,t) + \lambda_b^{\,2} w^{IV}(x,t) = -\ddot{Y}(t) \qquad (6)$$

(7)

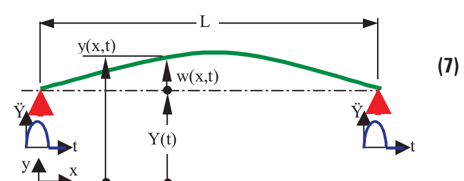

Figure 2: PCB modelled as an Euler-Bernoulli beam

Drop Impact: Fundamentals and Impact Characterisation of Solder Joints (cont.)

where $\lambda_b^2 = D_b/\rho h$ and $D_b = EI$ is the flexural stiffness of the PCB as a beam. The bending moment and acceleration along the PCB as a function of time have been derived as a superposition of flexing modes [11] and are presented in eq(7a) and eq(7b) respectively.

(7a)
$$\frac{\omega_1^2 L^2}{\pi^2 A_o}\frac{M(x,t)}{EI} = \sum_{n=1,3}^{\infty}\frac{-4}{\pi n^3}.T(R_\omega,t).\sin\frac{n\pi x}{L}$$

(7b)
$$\frac{\ddot{y}(x,t)}{A_o} = \sum_{n=1,3}^{\infty}\frac{-4}{n\pi}\left[T(R_\omega,t)+\sin\Omega t\right]\sin\frac{n\pi x}{L}+\sin\Omega t \quad \text{for } t \le t_o$$
$$= \sum_{n=1,3}^{\infty}\frac{-4}{n\pi}.T(R_\omega,t).\sin\frac{n\pi x}{L} \quad \text{for } t \ge t_o$$

The function $T(R_\omega,t)$ is given by eq(8).

(8)
$$T(R_\omega,t) = \frac{R_\omega}{1-R_\omega^2}(R_\omega \sin\omega t - \sin\omega t) \quad \text{for } t \le t_o$$
$$= \frac{-2R_\omega}{1-R_\omega^2}\sin\left(\omega t - \frac{\pi R_\omega}{2}\right)\cos\left(\frac{\pi R_\omega}{2}\right) \quad \text{for } t \ge t_o$$

where ω_1 is the fundamental flexing frequency of the PCB, and $R_\omega = \omega_n/\Omega$ is the ratio of n-mode PCB flexing frequency to the frequency of the base acceleration.

Similar expression for PCB modelled as a thin rectangular plate simply supported at its edges is provided, without elaboration, in eq(9 & 10) [11].

(9)
$$\ddot{w}(x,y,t)+\lambda_p^2\nabla^4 w(x,t) = -\ddot{Z}(t)$$

(10a)
$$\frac{\omega_1^2 a^2}{\pi^2 A_o}\frac{M_x(x,y,t)}{D_p} = \sum_{\substack{n=1,3,5\\m=1,3,5}}^{\infty}\frac{-16}{\pi^2 nm}\left(n^2+\frac{\nu m^2}{s^2}\right)\left(\frac{1+s^2}{s^2n^2+m^2}\right)^2 T(R_\omega,t)\sin\left(\frac{n\pi x}{a}\right)\sin\left(\frac{m\pi y}{b}\right)$$

(10b)
$$\frac{\ddot{z}(x,y,t)}{A_o} = \sum_{\substack{n=1,3,5\\m=1,3,5}}^{\infty}\frac{-16}{nm\pi^2}\left[T(R_\omega,t)+\sin\Omega t\right]\sin\frac{n\pi x}{a}\sin\frac{n\pi y}{b}+\sin\Omega t \quad \text{for } t \le t_o$$
$$= \sum_{\substack{n=1,3,5\\m=1,3,5}}^{\infty}\frac{-16}{nm\pi^2}T(R_\omega,t)\sin\frac{n\pi x}{a}\sin\frac{n\pi y}{b} \quad \text{for } t \ge t_o$$

where $\lambda_p^2 = D_p/\rho h$ and $D_p = Eh^3/12(1-\nu^2)$ is the flexural stiffness of PCB as a plate; a and s are the length and width-to-length ratio of the PCB respectively.

These equations have been implemented into a simple numerical program and have been validated against FE analysis [11]. The response spectrum of bending moment and acceleration at the centre of PCB, modelled as a thin plate with s=1, is illustrated

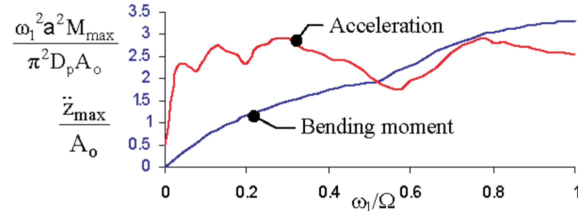

Figure 3: Response spectrum of acceleration and bending moment at the centre of PCB

in Fig 3.

2.3 Interconnection stress due to board bending

The bending moment in the PCB induces flexing of the PCB. But the IC component that is attached to the PCB does not acquire the same curvature as the PCB due to the different boundary condition. This differential flexing curvature induces stresses on the solder interconnection. This is illustrated in Fig 4(a). The stress in the interconnection may be modelled analytically using beam on elastic foundation technique [12] whereby the interconnections are modelled as a continuous elastic foundation (Fig 4b) that transmits only axial force across the PCB and the IC component. The bending moment, Mb, is applied along the edges of the PCB. The uniform axial stress in a discrete interconnection at distance Γ from the middle of the IC component can be shown to be

(11)
$$S(\Gamma) = \frac{M_b.k_a.A_r}{2\gamma^3 D_{pcb}}\left[(\chi+\varphi)\xi_3+(\chi-\varphi)\xi_4\right]_{\Gamma-p/2}^{\Gamma+p/2}$$

Drop Impact: Fundamentals and Impact Characterisation of Solder Joints (cont.)

where $\gamma = \sqrt[4]{k_a / 4D_e}$ is a characteristic parameter, k_a is the axial stiffness of the elastic foundation per unit length per unit width, D_e is the effective flexural stiffness of the PCB and IC package, given by $1/D_e = 1/D_{pcb} + 1/D_{pkg}$, A_r the ratio of the package area to the total area of the interconnections, p the interconnection pitch, $\xi_3 = \sinh(\gamma x)\cos(\gamma x)$, $\xi_4 = \cosh(\gamma x)\sin(\gamma x)$

$$\chi = \frac{\cosh\mu\sin\mu - \sinh\mu\cos\mu}{\sinh 2\mu + \sin 2\mu}, \varphi = \frac{\cosh\mu\sin\mu + \sinh\mu\cos\mu}{\sinh 2\mu + \sin 2\mu}, \mu = \gamma.L_p.$$

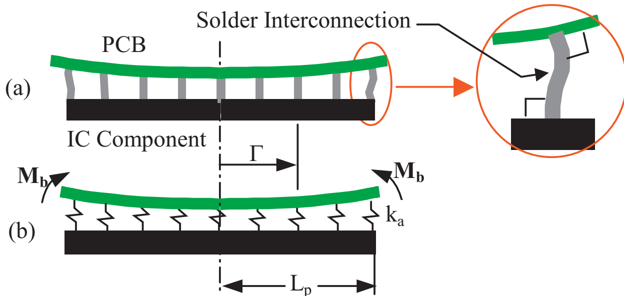

Figure 4: (a) Deformation of solder interconnection due to differential flexing; (b) beam on elastic foundation model

The inertial stress due to the accelerations of the IC package and its solder interconnections can be computed simply using D'Alembert's Principle. It can be readily shown that the interconnection stress due to board bending is 2 orders of magnitude higher than that due to acceleration [5, 11]. The role of flexing has been demonstrated in an experiment using a single daisy-chained CSP mounted at the centre of a PCB subjected to standard drop test [6,7]. The fibre strain measurement on the PCB shows the flexing of PCB consisting of fundamental mode superimposed with the next higher mode (Fig 5). The electrical connectivity became "open" after the PCB has flexed more than 30% of the amplitude corresponds to the fundamental bending mode. This was interrupted by momentary closure of the circuit that corresponds in time with the higher bending mode. The one-to-one correspondence of electrical connectivity and the fibre strain endorses board bending as the dominant failure driver.

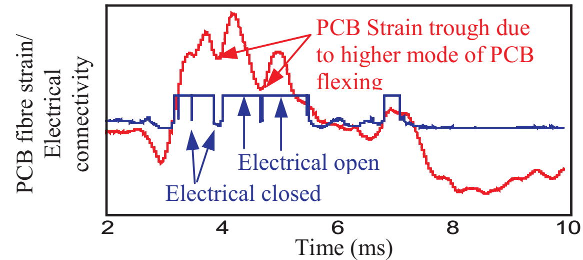

Figure 5: One-to-one correspondence of PCB flexing and electrical connectivity

3. Impact Characterisation of Solder Joints

The structural integrity of the interconnection under drop impact depends not only on the magnitude of the driving force, but also the resistance of the materials. Component level material testing is highly desirable, especially for quality assurance, due to its low cost. However, the prevailing industry practice of solder ball shearing is inappropriate due to its slow speed which tends to induce failure only in the bulk solder while not evaluating the more critical intermetallic (IMC) region.

The characterisation work by [14] using split Hopkinson bar technique has provided evidence of ductile-bulk solder to brittle-IMC failure transition for pristine ternary Pb-free solder ball on electroless Ni-P/Au (ENIG) pad finishing when the shear speed was raised from 1 mm/min to 3 m/s. At the shear speed of 3 m/s, the Sn3.8Ag0.7Cu solder alloy exhibited only a third of the fracture strength of Sn37Pb solder alloy. Similar ductile-bulk to brittle-IMC failure was also reported by [15] using miniature Charpy when the shear speed was raised from 0.2 mm/s to 1 m/s. At the shear speed of 1 m/s, Sn3Ag0.5Cu solder, on both Cu-organic surface preservative (OSP) and ENIG pad finishing, was found to have a third higher fracture energy than the Sn37Pb solder alloy.

A possible reason for the discrepancy is that the two works did not measure the same characteristic – one measuring fracture strength while another measuring fracture energy. The following works investigate the component level characteristics of solder balls in details using Instron Micro Impactor which gives both fracture strength and fracture energy.

Drop Impact: Fundamentals and Impact Characterisation of Solder Joints (cont.)

3.1 Experiment

The sample consists of ϕ400µm solder ball on organic substrate. The test matrix consists of 5 solder alloys, 4 pad finishes, 3 thermal histories, and 2 solder mask designs forming a total of 120 combinations. Each combination consists of at least 11 specimens, 5 of which were evaluated under static shearing and the rest under impact shearing. The details are tabulated in Table 1.

Solder alloys	▪ Sn37Pb ▪ Sn3.5Ag ▪ Sn3.8Ag0.7Cu ▪ Sn2.5Ag0.8Cu0.5Sb ▪ Sn58Bi
Pad finishes	▪ Electroless Ni-P/Au (ENIG) ▪ Hot air Sn37Pb solder levelling (HASL) ▪ Organic surface preservative (OSP) ▪ Immersion tin (Tin)
Thermal histories	▪ As-reflow (pristine) ▪ Thermal aging at 125^0C for 125 hrs (Aged) ▪ Temperature cycle -40^0C to 125^0C with 15 mins dwell and 15 mins ramp for 500 cycle (TC)
Mask design	▪ Solder mask defined with ϕ500µm pad and ϕ300µm pad opening (SMD) ▪ Non-solder mask defined with ϕ300µm pad and ϕ500µm mask opening (NSMD)
Shear speed	▪ 50µm/s using Dage BT100 (Static) ▪ 600 µm/s using Instron Micro Impactor (Impact)

3.2 Results

Static Fracture Strength

Fig 6a depicts the static shear fracture load for SMD design, pristine condition, (SMD_pristine) for the full combination of solder alloys and pad finishes and Fig 6b depicts the percentage variation of fracture load after thermal aging and temperature cycling (TC) respectively. The following observations may be made: (i) There is no significant differences among the solder alloys except for SnBi solder which exhibits significantly higher fracture strength. (ii) Both aging and TC reduces the static fracture strength, though it varies significantly with respect to pad finishing. (iii) The specific combination of SnBi solder with HASL pad finish exhibits a huge reduction in fracture strength. This is believed to be attributed to the formation of low-melting point ternary SnBiPb eutectic phase [16] when Bi from solder ball alloys with SnPb from pad finishing.

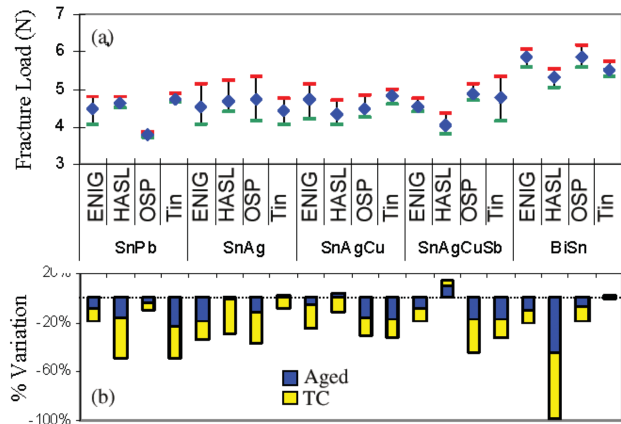

Figure 6: Static fracture strength of SMD (a) pristine (b) aged and TC

Impact Fracture Strength & Fracture Modes

The impact fracture load of SMD_pristine system together with fracture modes are depicted in Fig 7a. Observations: (i) The impact fracture strength of solder joint is generally higher than its static fracture strength. (ii) The impact fracture strength exhibits higher dispersion in data. (iii) SnAg solder exhibits the highest while BiSn solder the lowest impact fracture strength. (iv) SnPb solder exhibits predominantly bulk failure – failure usually occurs just beneath the shear tool. Pb-free solder, on the other hand, exhibit predominantly a mixture of IMC and bulk failure – failure usually occurs along the bond interface. Note that in most cases even though the failure surface appeared visually as brittle IMC, this was at times accompanied by traces of tin picked up by EDS. The definition of "IMC + bulk" use here therefore encompasses failure in the IMC as well as between IMC and the solder interface.

The effect of thermal treatment is depicted in Fig 7b. Note that while aging induces diverse response from various solder alloys, TC tends to reduce the impact fracture strength of all solder alloys. Note again the huge reduction in impact fracture strength for the specific combination of BiSn solder with HASL pad finishing.

Drop Impact: Fundamentals and Impact Characterisation of Solder Joints (cont.)

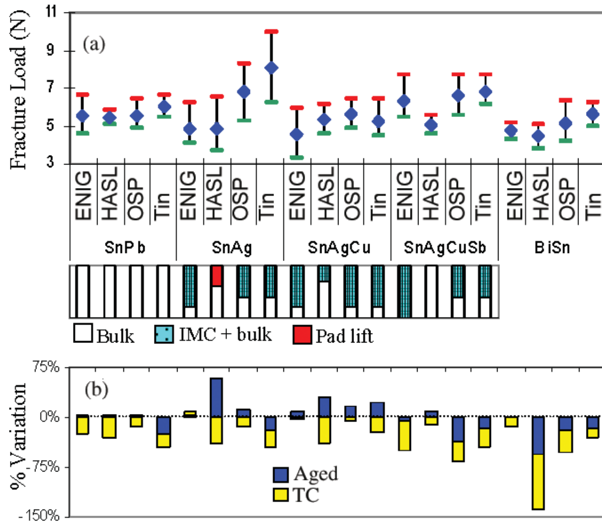

Figure 7 Impact fracture strength of SMD (a) pristine (b) aged and TC

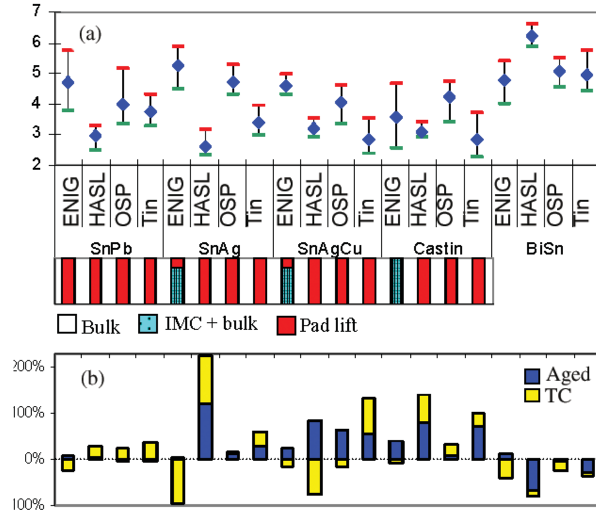

Figure 8 Impact fracture strength of NSMD (a) pristine (b) aged and TC

The fracture load of NSMD-pristine system is depicted in Fig 8. Observations: (i) The fracture strength is generally lower than that of SMD_pristine – similar observation was also made for static shear. (ii) The fracture strength fluctuates wildly with pad finishing. (iii) The filure mode is predominantly "pad-lift" which could explain the lower fracture strength. (iv) Interestingly, the fracture strength seems to follow, despite vaguely, the reverse trend of the melting temperature of the solder alloys. (v) The system has in general benefited from thermal treatment, but the response differs significantly between solder alloys and pad finishing.

Force-Time characteristic

The force-time history of the impact is fully registered by the Micro Impactor. The force-time characteristics of typical SMD_pristine system are depicted in Fig 9. With known velocity of the impact head, the force-time characteristic can be readily transformed into force-displacement characteristic and the energy consumed in fracturing the solder ball can be computed. It is observed that the SnPb solder while not giving absolutely high fracture load tends to give high fracture displacement with resultant high fracture energy.

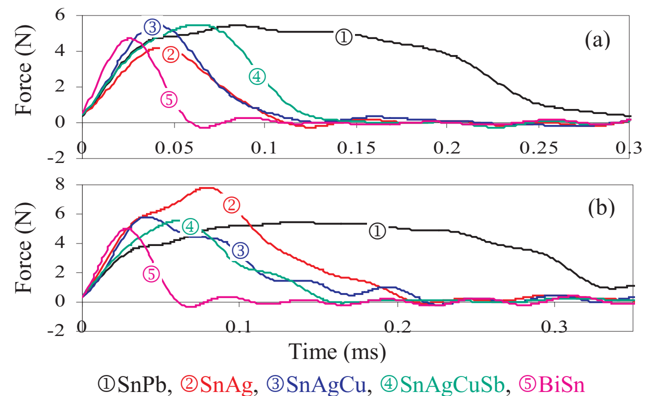

Figure 9 Typical force-time characteristics for SMD_pristine system (a) ENIG (b) OSP

Drop Impact: Fundamentals and Impact Characterisation of Solder Joints (cont.)

Impact Fracture Energy

The fracture energy of SMD system is depicted in Fig 10. Observations: (i) SnPb solder exhibits the highest fracture energy follows by SnAg solder with BiSn solder exhibiting the least fracture energy. (ii) The dispersion of data is much more than that observed for fracture strength. (iii) Thermal treatment gave rise to diverse effect for the system.

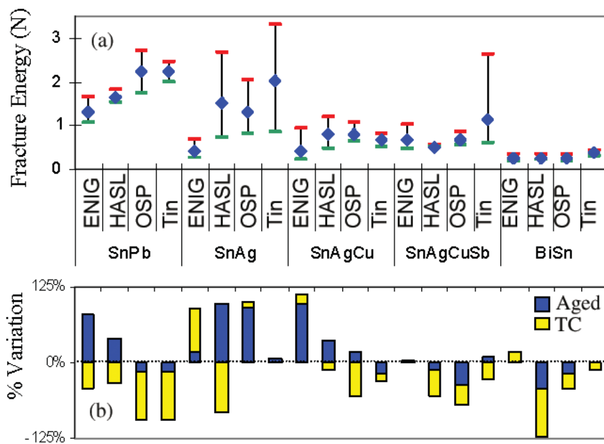

Figure 10 Impact fracture energy of SMD (a) pristine (b) aged and TC

Summary of Results

Fig 11 presents the average value (over all pad finishing) of static fracture strength, impact fracture strength, and impact fracture energy for individual solder normalised by the corresponding average value of SnPb solder. The solders are arranged in orders of increasing impact fracture strength. Observations: (i) SnAgCu solder while having comparable impact fracture strength as SnPb solder, has much lower impact fracture energy. (ii) SnAg solder seems to have the best impact characteristics, especially after thermal treatment. (iii) BiSn solder while having the highest static fracture strength has the lowest impact fracture strength and fracture energy.

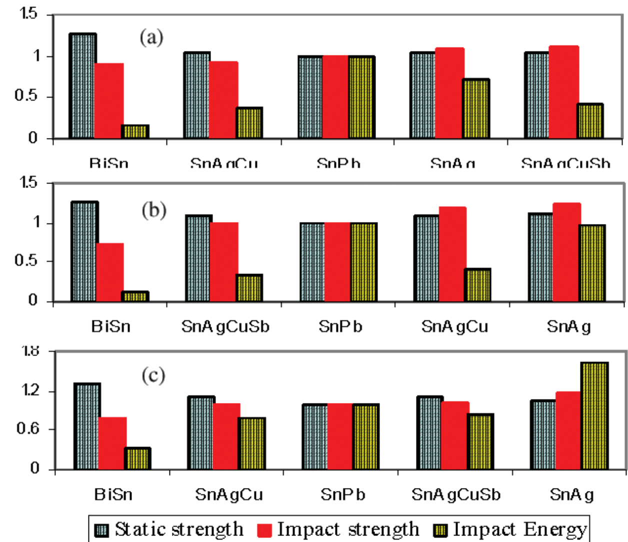

Figure 11 Summary SMD_solder (a) pristine (b) aged (c) TC

Fig 12 presents the average value (over all solder alloys) of static fracture strength, impact fracture strength, and impact fracture energy for individual pad finishing normalised by the corresponding average value of ENIG finishing. The finishing are arranged in orders of increasing impact fracture strength. In general, OSP and Tin finishing seems to outperform ENIG and HASL in terms of both impact fracture strength and impact fracture energy.

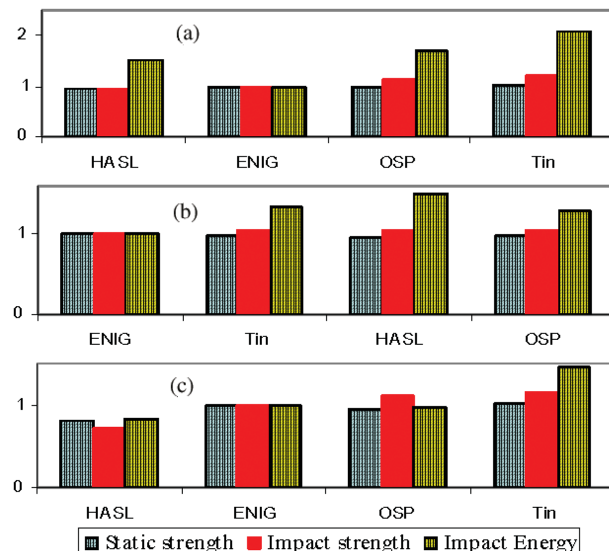

Figure 12 Summary SMD_pad (a) pristine (b) aged (c) TC

Drop Impact: Fundamentals and Impact Characterisation of Solder Joints (cont.)

Fig 13 presents the same for NSMD_pristine system. Observations: (i) There is no clear winner among the solders which is understandable in view of the fact that most of the failure is in the core material - manifested as pad-lift. (ii) Tin and HASL finishing seems to perform consistently poorer.

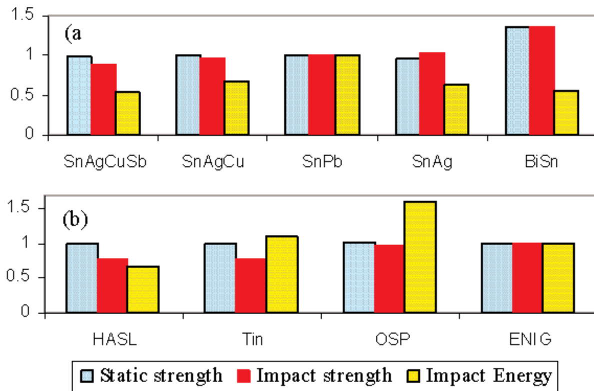

Figure 13: Summary NSMD_pristine system (a) solder (b) pad finishing

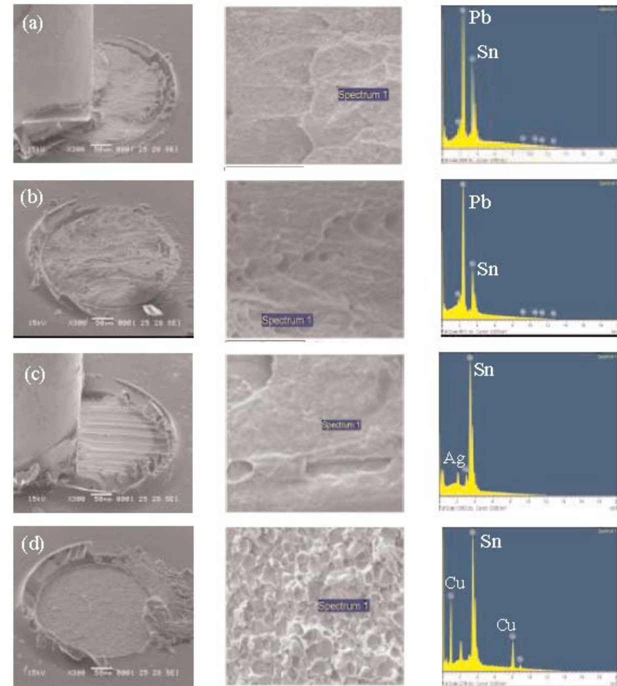

Figure 14: Fractographs of SMD_pristine SnPb_OSP subjected to (a) static shear, (b) impact shear; SnAgCu_OSP subjected to (c) static shear, (d) impact shear

Fractographs

Fig 14 presents the typical fractographs of SMD_pristine system for SnPb_OSP and SnAgCu_OSP subjected to static and impact shearing. Note (i) the ductile bulk solder failure in the SnPb_OSP system in both static and impact shearing, and (ii) the ductile bulk solder to brittle IMC transition in the SnAgCu_OSP system with increased shearing speed. Fig 15 presents the typical fractographs of NSMD_pristine system for the same solder_finishing and loadings. Bulk solder failure were observed in both systems under static shearing while core material failure were observed in both systems under impact shearing.

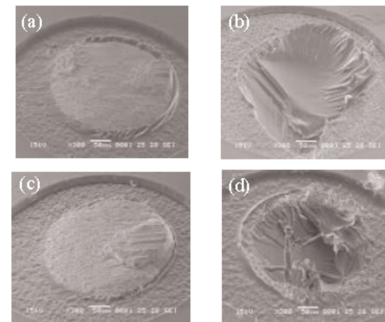

Figure 15: Fractographs of NSMD_pristine SnPb_OSP subjected to (a) static shear, (b) impact shear; SnAgCu_OSP subjected to (c) static shear, (d) impact shear

Drop Impact: Fundamentals and Impact Characterisation of Solder Joints (cont.)

4. Discussions

Fracture Strength Vs Shear Speed

The fracture characteristic of the solder joint with respect to shear speed may be illustrated schematically in Fig 16. The fracture strength of the ductile bulk solder starts low but increases with shear speed while that of the brittle IMC or IMC-solder bond (for SMD system) or the core material (for NSMD system) starts high but decreases with shear speed. The fracture strength of solder joint follows that of the bulk solder at low speed and jumps to that of IMC or IMC-solder (or core materials for NSMD system) after the transition shear speed. It is clear that the fracture strength of the IMC and IMC-solder bond depends both on the types of solder as well as the pad finishing. In the case of fine interconnection pitch when the solder volume is small, the fracture strength of the bulk solder may also depend to a small degree on the pad finishing through diffusion of pad metallurgy into the bulk solder.

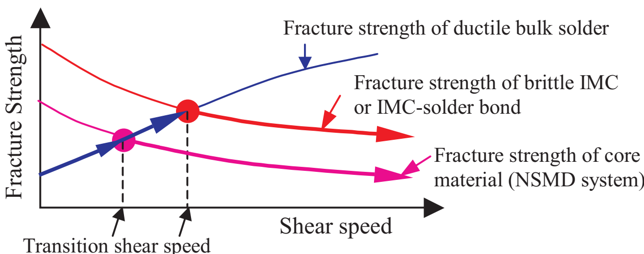

Figure 16: Summary SMD_solder (a) pristine (b) aged (c)

Fracture Strength & Fracture Energy

The bulk solder, IMC, IMC-solder bond, and the core material of the organic laminate shall have adequate fracture strength and impact toughness (expressed in terms of fracture energy) such that the board level interconnection does not experience catastrophic failure in just a single drop. At the same time, high fracture strength and fracture toughness are also believed to be desirable for the board level interconnection to survive the hundreds of flexing cycles experienced in the 30 repeated drops specified in JEDEC Std JESD22-B111 [1].

SMD Vs NSMD

Compared to SMD system, NSMD system exhibits significantly lower impact fracture strength and energy. This is partly attributed to the absence of reinforcement from the solder mask in the NSMD system and partly due to the stress concentration along the edge of the pad that led to cracking and cratering of underneath core material. Such failure is going to be more prevalent with decreasing pad size and is potentially a limiting factor to decreasing interconnection pitch.

SnAgCu Vs SnPb

In view of the pad-lift failure nature of NSMD system, comparison between SnAgCu and SnPb solders were made only using SMD system. While there is little difference between the impact fracture strength of both solders, the impact toughness of SnAgCu solder is much lower than that of SnPb solder. While it is not clear at this point the relative role of fracture strength and fracture energy in the drop impact reliability of solder interconnection, it is reasonable to believe that the drop impact reliability of SnAgCu solder is inferior to that of SnPb solder. Among the solders evaluated, it appears that SnAg solder possess the best characteristics for drop impact application.

The Ideal Pad Finishing

It appeared that OSP and Tin finishing compares favourably with HASL and ENIG finishing for SMD system. On the other hand, OSP and ENIG appear to be favoured for NSMD system. Since failure predominantly occurs in the core materials for the NSMD system, the poorer performance of Tin and HASL finishing is believe to be attributed to the high processing temperature that has resulted in degradation of the core materials. This argument may drawn support from the evidence that the impact fracture strength of solder alloys appeared to decline with solders that have increasing melting (hence processing) temperature (Fig 8). However, in view of the large standard deviation of the data, one needs to treat these deduction with care until further supporting evidence.

Drop Impact: Fundamentals and Impact Characterisation of Solder Joints (cont.)

Component level QC test

It is clear that the component level ball impact shear test can not introduce a similar state of loading on the board level interconnection as in a JEDEC prescribed board level drop impact test. However being simpler and cheaper to perform, it has the potential as a quality control tool for component manufacturing. As a QC tool, it is only important that the impact test is able to induce failure in the weakest element as observed in the JEDEC test. For example, if the observed weakest element in the JEDEC test for SnPb solder is the bulk solder while that in the Pb-free solder is the IMC bond interface, the component level impact shear test shall be able to evaluate these weak elements qualitatively – by producing similar fracture mode. In the same argument, the appropriate impact shear speed shall be the speed that can induce failure in the weakest element.

5. Conclusion

A summary of the fundamental mechanics behind a board level drop impact test has been presented with analytical equations provided for the dynamics of the JEDEC board level drop test, the dynamics of the PCB, as well as the interconnection stress.
A comprehensive study of the impact characteristics of the solder ball at component level has been performed using the newly developed Micro Impactor that provides both the fracture strength and fracture energy. The following conclusions has been drawn:

- SMD design is stronger than NSMD design.
- The impact characteristic of Sn3.8Ag0.7Cu solder is inferior while the Sn3.5Ag solder is superior to that of Sn37Pb solder.
- OSP and Tin pad finishing performed well for SMD system while OSP and ENIG finishing performed well for NSMD system.
- Both impact strength and impact energy are important to prevent catastrophic and cyclic failure of board level interconnection.
- The drop impact reliability of the solder joint shall be evaluated at the speed that induces the appropriate failure mode.

6. Acknowledgements

The authors would like to acknowledge the excellent work of internship student Raj Kumar of Ngee Ann Polytechnic.

Symbols

a, L, L_p: Length of plate, beam, half length of the IC package
A_o, t_o: Amplitude, duration of half-sine base acceleration
A_r: Ratio of package area to the area of the interconnection
D_b, D_p: Flexural stiffness of beam, plate
D_{pcb}, D_{pkg}, D_e: Flexural stiffness of PCB, IC package, effectiveness stiffness of PCB and package modeled as beam
E, h, I, ρ, ν: Modulus, thickness, moment of inertia, density, Poisson ratio of PCB/package
H: Free-fall height
k_a, k, K: Axial stiffness of continuous interconnection, linear stiffness of PCB, linear stiffness of shock pad
m, M: Concentrated mass of PCB, base
M_b, $M(x,t)$, $M(x,y,t)$: Bending moment in beam, plate
p: Interconnection pitch
$S(\Gamma)$: Axial stress in the discrete interconnection
V_o: Impact velocity
$w(x,t)$, $w(x,y,t)$: Deflection of beam, plate with respect base
$y(x,t)$, $z(x,y,t)$: Displacement of beam, plate with respect to an absolute reference
$Y(t)$, $Z(t)$: Displacement of base
ω_n: The nth angular modal frequency of vibrating body
Ω: Angular frequency of input base acceleration

References

[1] JEDEC Standard JESD22-B111, “Board level drop test method of components for handheld electronic products”.
[2] S.K.W. Seah, et al., "Mechanical response of PCBs in portable electronic products during drop impact," Proc 4th EPTC, Singapore, pp. 120-125, 2002.
[3] C.T. Lim, et al., “Drop impact survey of portable electronic products”, Proc 53rd ECTC, 2003.
[4] E.H. Wong, et al., “Tackling board level drop impact reliability of electronic interconnections”, Interpack 2003.

Drop Impact: Fundamentals and Impact Characterisation of Solder Joints (cont.)

[5] E.H. Wong, et al., "Drop impact test – Mechanics & physics of failure", Proc 4th EPTC, pp. 327-333, 2002.
[6] E.H. Wong, et al., "Fundamentals of drop impact", presented in JEDEC working group meeting, Dec 2003.
[7] S.K.W. Seah, at al., "Experiments and failure drivers in drop impact of portables", JEDEX, San Jose, 2004
[8] T. Sogo, et al., "Estimation of fall impact strength for BGA solder joints", Proc. ICEP, pp. 369-373, 2001.
[9] L. Zhu, "Submodeling technique for BGA reliability analysis of CSP packaging subjected to an impact loading", Proc. IPACK, 2001.
[10] J. Wang, et al., "Modeling solder joint reliability of BGA packages subject to drop impact loading using submodelling", Proc. Abaqus Conference, 2002.
[11] E.H. Wong, "Dynamics of board level drop impact", ASME Trans. JEP, to be published in Jul issue 2005.
[12] E. Suhir, "On a paradoxical phenomenon related to beams on elastic foundation: Could external compliant leads reduce the strength of a surface-mounted device?", J. Applied Mechanics, 55:818, 1988.
[13] M.A. Meyers, "Dynamic behavior of materials", John Willey, 1994.
[14] D.M. Williamson, et al., "Spall, quasi-static and high strain rate shear strength data for electronic solder materials", Internal report Cavendish Laboratory No. SP 1113, Oct 2002.
[15] M. Date, et al., "Impact reliability of solder joints", Proc 54 ECTC, pp. 668-674.
[16] J. Bath, et al., "Research update: lead-free solder alternatives", Circuit Assembly, May 2000 issue.